

# Beam–Beam Effects in Linear Colliders

*D. Schulte*

CERN, Geneva, Switzerland

## Abstract

Linear colliders are promising candidates for future high-energy lepton colliders. Two options are studied in global collaborations, the International Linear Collider (ILC) and the Compact Linear Collider (CLIC). Beam–beam effects are an important driver of linear collider design choices and they affect the performance of physics experiments. The lecture introduces the main physics relevant for the beam collision and the impact on the parameter choice.

## Keywords

Linear Collider; beam-beam; pinch effect; beamstrahlung; ILC; CLIC.

## 1 Linear colliders

To date only one linear collider has been operated for physics, the Stanford linear collider (SLC) (no definitive reference is available for the SLC, but one can use the report [1] and the references therein as a starting point). It has been operated at the Z-resonance. Two future linear collider projects are under consideration, the International Linear Collider (ILC [2–6]) and the Compact Linear Collider (CLIC [7,8]). The ILC aims at a centre-of-mass energy of 500 GeV, potentially starting at 250 GeV. The CLIC is foreseen to be implemented in three stages ranging from a centre-of-mass energy of 380 GeV up to 3 TeV.

In circular electron–positron colliders synchrotron radiation becomes a severe issue as the beam energy increases, since the radiation power increases with the fourth power of the energy. This can be avoided in linear colliders. A generic example of a linear collider is shown in Fig. 1. The beams are produced in an electron and a positron source, respectively. They are slightly accelerated and transported to a damping ring. Here their emittance is reduced to very small values, especially in the vertical plane. Then the beams are transported through the ring to main linac system (RTML). During the transport they are slightly more accelerated and compressed longitudinally. In the main linac they are accelerated to full energy. In the beam delivery system (BDS) the beams are then focused to very small sizes at the collision point. Then they are disposed of in beam dumps.

The main challenges of a linear collider are first to achieve the beam energy in the main linac. This requires very high gradients for the acceleration. The second challenge is to achieve the high luminosity in a single pass. This requires very dense beams at the collision point. Both ILC and CLIC will deliver short pulses of bunches that collide with longer intervals between pulses.

The ILC is based on the use of superconducting cavities to accelerate the beams. These allow the use of long beam pulses. To provide the accelerating field, the cavity needs to be filled with energy. This energy is lost very slowly in the walls of the cavity and hence one can afford a long pulse. In contrast, the CLIC is based on high-gradient normal-conducting accelerating structures. These require very short pulses, since the energy in the accelerating structures is lost rapidly in the copper walls. To achieve sufficient efficiency it is therefore necessary to use very short pulses and to increase the beam current in the pulse as much as possible. This requires short distances between the bunches. The advantage of the normal-conducting accelerating structures is that they allow us to use higher accelerating fields than superconducting cavities (a factor of about three between CLIC and ILC). To achieve multi-TeV energies at practical machine length and cost thus requires the use of normal-conducting technology. The main beam parameters for linear colliders are given in Table 1.

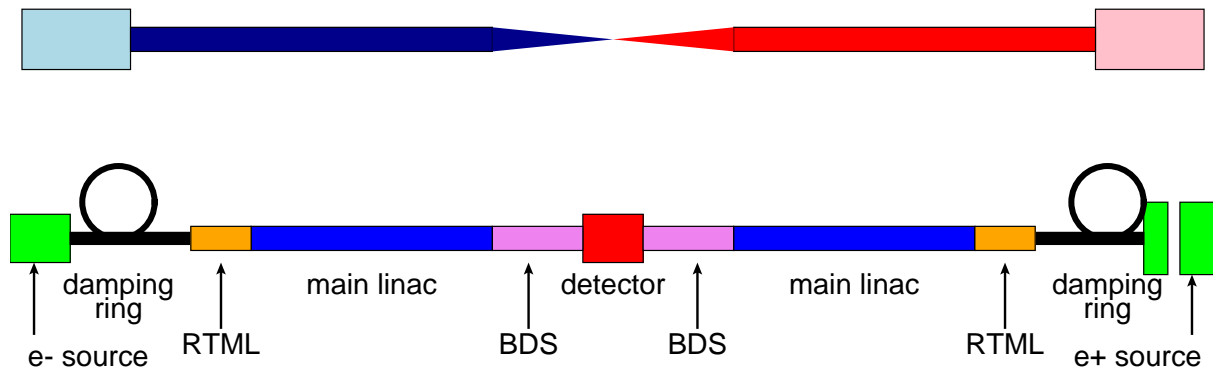


**Fig. 1:** Generic layout of a linear collider. The beams are illustrated at the top. They are produced with relatively large emittances, which are then reduced in the damping rings. From there to the interaction point the emittances increase somewhat before the beams are focused at the interaction point.

**Table 1:** The main parameters of SLC, ILC and CLIC. More parameter sets exist for ILC and CLIC at different energies. The CLIC set at 3 TeV includes the higher order optics and radiation effects in the beam delivery system.

Parameter	Symbol [unit]	SLC	ILC	CLIC	CLIC
Centre-of-mass energy	$E_{\text{cm}}$ [GeV]	92	500	380	3000
Geometric luminosity	$\mathcal{L}_{\text{geom}}$ [ $10^{34} \text{ cm}^{-2} \text{ s}^{-1}$ ]	0.00015	0.75	0.8	4.3
Total luminosity	$\mathcal{L}$ [ $10^{34} \text{ cm}^{-2} \text{ s}^{-1}$ ]	0.0003	1.8	1.5	6
Luminosity in peak	$\mathcal{L}_{0.01}$ [ $10^{34} \text{ cm}^{-2} \text{ s}^{-1}$ ]	0.0003	1	0.9	2
Gradient	$G$ [ $\text{MV m}^{-1}$ ]	20	31.5	72	100
Particles per bunch	$N$ [ $10^9$ ]	37	20	5.2	3.72
Bunch length	$\sigma_z$ [ $\mu\text{m}$ ]	1000	300	70	44
Collision beam size	$\sigma_{x,y}$ [ $\text{nm nm}^{-1}$ ]	1700/600	474/5.9	149/2.9	40/1
Emittance	$\epsilon_{x,y}$ [ $\mu\text{m nm}^{-1}$ ]	3/3000	10/35	0.95/30	0.66/20
Beta function	$\beta_{x,y}$ [ $\text{mm mm}^{-1}$ ]	100/10	11/0.48	8.2/0.1	6/0.07
Bunches per pulse	$n_b$	1	1312	352	312
Distance between bunches	$\Delta z$ [ns]	—	554	0.5	0.5
Repetition rate	$f_r$ [Hz]	120	5	50	50
Horizontal disruption	$D_x$	0.6	0.3	0.24	0.2
Vertical disruption	$D_y$	1.7	24.3	12.5	7.6
Photons per beam particle	$n_\gamma$	—	1.9	1.5	2.1
Average photon energy	$\langle E_\gamma/E_0 \rangle$ [%]	—	2.4	4.5	13
Coherent pairs	$N_{\text{coh}}$ [ $10^8$ ]	—	—	—	6.8
Their energy	$E_{\text{coh}}$ [ $10^8 \text{ TeV}$ ]	—	—	—	2.1
Incoherent pairs	$N_{\text{incoh}}$ [ $10^3$ ]	—	196	58	300
Their energy	$E_{\text{incoh}}$ [TeV]	—	484	187	$2.3 \times 10^4$

## 2 Luminosity and parameter drivers

The luminosity target for linear colliders is around  $10^{34} \text{ cm}^{-2} \text{ s}^{-1}$  following the requests of the experiments. In Table 1, one can note that ILC and CLIC use flat beams to achieve this ambitious luminosity target and that the vertical beam size is only of the order of a nanometre. In the following we will discuss the reason for this.

The luminosity  $\mathcal{L}$  in a linear collider is given by the following formula:

$$\mathcal{L} = H_D \frac{N^2}{4\pi\sigma_x\sigma_y} n_b f_r. \quad (1)$$

Here,  $N$  is the number of particles per bunch,  $\sigma_{x,y}$  are the horizontal and vertical beam sizes at the collision point,  $n_b$  is the number of bunches per train,  $f_r$  is the rate of trains per second and  $H_D$  is a factor that contains the impact of beam–beam forces and other relevant effects. The factor  $H_D$  is typically in the order of 1.5–2. It is useful to rewrite the formula in the following form:

$$\mathcal{L} \propto H_D \frac{N}{\sigma_x\sigma_y} N n_b f_r. \quad (2)$$

The term  $N n_b f_r$  represents the beam current. Its upper limit arises from the power consumption of the collider and the efficiency to turn this power into beam power. It is therefore important to maximize the luminosity per beam current, i.e. the factor  $N/(\sigma_x\sigma_y)$ . However, a lower limit to the beam size arises from the beam–beam effects.

At collision, the beams are so dense that they generate very strong electromagnetic fields. In an electron–positron collider they focus each other; Fig. 2 illustrates this. In circular colliders this deflection is quite small and can be understood as a thin-lens kick. In a linear collider the beams are so dense that the particles move strongly during the collision. This so-called pinch effect reduces the effective beam size and leads to an increase in luminosity. It has been experimentally verified in the SLC [1], where under some conditions the luminosity was more than doubled. But this motion also leads to the emission of radiation, the so-called beamstrahlung, which alters the energy of the colliding beam particles. As a consequence the luminosity is not only provided at full beam energy but also at lower energies: a luminosity spectrum forms; see Fig. 2. This places some constraint on the beam parameters.

One can rewrite the luminosity formula further:

$$\mathcal{L} \propto H_D \frac{N}{\sigma_x} N n_b f_r \frac{1}{\sigma_y}. \quad (3)$$

In the following we will see that the term  $N/\sigma_x$  is related to the beamstrahlung emitted. Its upper limit is defined by the requirements of the physics experiments. The term  $1/\sigma_y$  finally is limited by the ability to achieve and preserve a small beam emittance and to squeeze the beam to a very small size.

## 3 Basic beam–beam effects

In the following we discuss the fundamentals of the pinch effect and the beamstrahlung. We will discuss head-on collisions even if the beams collide at an angle. The angle can however be neglected because in the proposed designs it is compensated by crab crossing.

### 3.1 Pinch effect

#### 3.1.1 Disruption

The focusing effect of the colliding electron and positron bunches can be described by the so-called disruption parameter. First, let us assume that the effect is so weak that the particles receive a transverse kick during the passage of the oncoming bunch but that they do not change their positions. If a particle

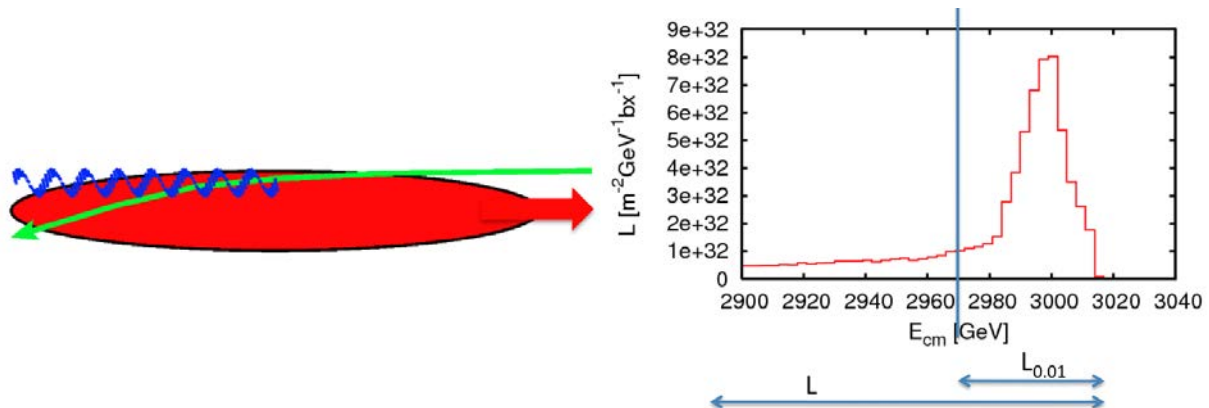


**Fig. 2:** Left: an electron is deflected by the fields of the oncoming bunch and emits a beamstrahlung photon. Right: the luminosity spectrum in CLIC at 3 TeV. The part of the luminosity above 99% of the nominal centre-of-mass energy is called  $\mathcal{L}_{0.01}$ . Values are given as integrated luminosity per energy band and bunch crossing (bx).

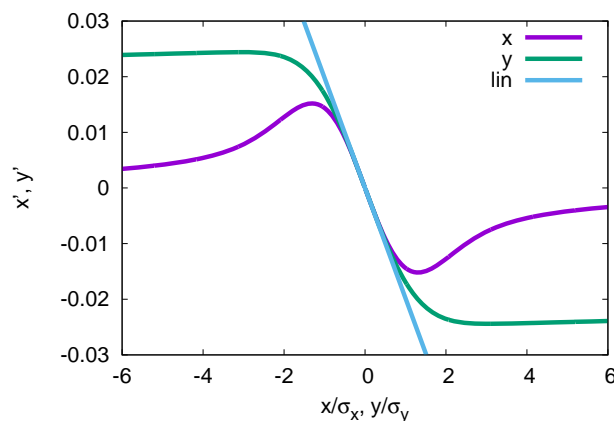


**Fig. 3:** The deflection of particles due to the fields of the oncoming bunch

is close to the centre of the beam, the deflection will depend linearly on the offset, while it will grow less than linearly and even become smaller at larger offset. See Fig. 3 for an example of a very flat beam. One can easily calculate the deflection of a particle in the linear regime:

$$\left. \frac{dx}{dz} \right|_{\text{final}} = \frac{2Nr_e}{\gamma\sigma_x(\sigma_x + \sigma_y)} x, \quad \left. \frac{dy}{dz} \right|_{\text{final}} = \frac{2Nr_e}{\gamma\sigma_y(\sigma_x + \sigma_y)} y.$$

Here,  $r_e \approx 2.8$  fm is the classical electron radius and  $\gamma$  is the relativistic factor of the particles. In each plane, the core of the beam is thus focused into one point with a distance  $f_{x,y}$  after the collision point. We define the disruption parameters  $D_{x,y} = \sigma_z/f_{x,y}$ . Hence,

$$D_x = \frac{2Nr_e\sigma_z}{\gamma\sigma_x(\sigma_x + \sigma_y)}, \quad D_y = \frac{2Nr_e\sigma_z}{\gamma\sigma_y(\sigma_x + \sigma_y)}.$$

For  $D_{x,y} \ll 1$ , the particles will not move significantly during the collision, so our model is correct. For  $D_{x,y}$ , the motion during the collision will be large, so we need to take it into account. In linear colliders one typically finds that the horizontal disruption is small and the vertical disruption is large; see Table 1.

### 3.1.2 Simulation codes

For large disruption analytical models are difficult to develop and computer codes are used to simulate the effect. The two most widely used codes are GUINEA-PIG [10] and CAIN [9]. These codes represent

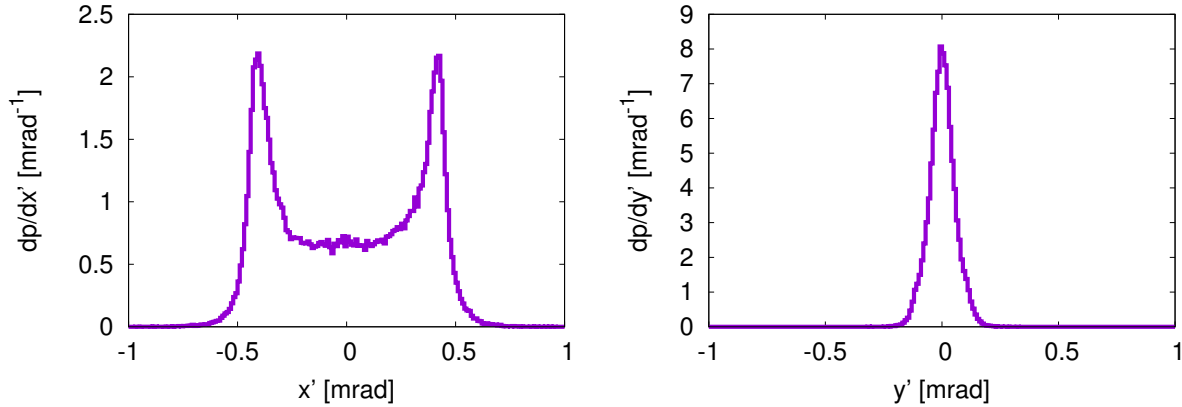


**Fig. 4:** The angular distribution of the particles of the spent beam

the beam by a number of macroparticles. Since the fields of the particles are transverse one can divide the two beams into slices. At any time, only the two slices of the beams which are at the same  $z$ -position can interact with each other. A particle is affected only by the fields of the other beam. After this interaction they are moved forward to interact with the next slice. The interaction within a slice can be treated as a two-dimensional problem of line charges, which can be solved using particles-in-cell or clouds-in-cell methods. The slices are divided transversely into cells by a grid. In the first step the charges are distributed over this grid. In the second step the fields at the grid points are computed. Using clouds, i.e. extended particles, instead of point-like particles helps to suppress high-frequency components that are an artefact of the finite resolution of the grid. In the third step the forces on each particle are calculated and the particles are moved forward. The grid is also used to calculate the luminosity. The particles of the two beams that are in the same cell collide with each other.

The codes also include the beamstrahlung effect, which is described in more detail below, and the generation of the different electron–positron background processes. GUINEA-PIG also includes the generation of hadronic background and the generation of muons; both processes will not be discussed here.

### 3.1.3 Typical results

Table 1 shows the luminosities for ILC and CLIC. The geometric value is calculated using the simplified formula

$$\mathcal{L}_{\text{geometric}} = \frac{N^2}{4\pi\sigma_x\sigma_y} n_b f_r. \quad (4)$$

The total luminosity is based on a full simulation of all beam–beam effects. The ratio of the two values is  $H_D$  and one can easily see that it is within the range of 1.5–2 as mentioned above.

The angular distribution of the spent beam is shown in Fig. 4 for the case of CLIC. In the detector design one has to take care to avoid that any of the beam particles can be lost inside the detector. However, the maximum angle of the particles is quite small; typically it is less than 1 mrad.

## 3.2 Beamstrahlung

When a particle is forced on a curved trajectory by the other beam, it will emit radiation in a similar fashion as in a bending magnet. This radiation is called beamstrahlung. For typical parameters each particle emits one to a few photons each of which carries some percentage of the particle’s energy. It is therefore important to be aware of the stochastic nature of the beamstrahlung. Due to beamstrahlung the particles lose energy during the collision and can therefore collide with less than the initial energy. This

leads to the formation of a luminosity spectrum. This obviously impacts the performance of the physics experiments. How important the effect is depends on the physics analysis that is being carried out.

The beamstrahlung can be described by its critical energy  $\hbar\omega_c$ , which can be calculated as

$$\hbar\omega_c = \frac{3}{2} \frac{\hbar\gamma^3 c}{\rho}. \quad (5)$$

Here,  $\rho$  is the bending radius of the particle trajectory. Conventionally one uses the so-called beamstrahlung parameter  $\Upsilon$ , which is defined as

$$\Upsilon = \frac{2}{3} \frac{\hbar\omega_c}{E}. \quad (6)$$

The beamstrahlung spectrum is described by the Sokolov–Ternov spectrum

$$\frac{d\dot{w}}{d\omega} = \frac{\alpha}{\sqrt{3}\pi\gamma^2} \left[ \int_x^\infty K_{5/3}(x') dx' + \frac{\hbar\omega}{E} \frac{\hbar\omega}{E - \hbar\omega} K_{2/3}(x) \right]. \quad (7)$$

Here,  $x = \frac{\omega}{\omega_c} \frac{E}{E - \hbar\omega}$  and  $K_{5/3}$  and  $K_{2/3}$  are the modified Bessel functions. In the limit  $\Upsilon \ll 1$  the power of the photon radiation of a particle is proportional to  $\Upsilon^2$ :

$$P = \frac{e^2}{6\pi\epsilon_0} \frac{c}{\rho^2} \gamma^4 = \frac{2}{3} \frac{r_e c}{\lambda_c^2} mc^2 \Upsilon^2 \quad (8)$$

with  $\lambda_c = \hbar/(mc)$ . The radiation spectrum of particles at different values of  $\Upsilon$  is shown in Fig. 5. The average beamstrahlung parameter can be estimated as

$$\langle \Upsilon \rangle = \frac{5}{6} \frac{Nr_e}{\alpha\sigma_z(\sigma_x + \sigma_y)}. \quad (9)$$

Here,  $\alpha$  is the fine structure constant. Conventionally one often omits the brackets. The maximum beamstrahlung parameter is about

$$\Upsilon_{\max} \approx \frac{12}{5} \Upsilon. \quad (10)$$

For  $\Upsilon \ll 1$ , the spectrum corresponds to synchrotron radiation and one speaks of the classical regime. For  $\Upsilon \gg 1$ , the radiation is partially suppressed since the critical energy is above the beam energy. This is the so-called quantum regime. Only CLIC at 3 TeV will operate in this regime.

As one can see in Table 1, all projects have a value of  $n_\gamma$  in the range of 1.5–2. The typical angular distribution of the photons is small, similar to the one of the beam particles after collision; see Fig. 6 for an example. Hence, the beamstrahlung does not generate direct background in the detector.

## 4 Choice of beam parameters

In this section, the choice of beam parameters at the collision point is described based on the beam–beam physics introduced above. We will focus on the case of classical beamstrahlung. For simplicity it is assumed that the bunch charge and length as well as the transverse emittances are already determined, e.g. by the main linac and other systems of the collider. This leaves the choice of beta functions and the longitudinal position of the waist. In reality the choice of parameters is more complex.

### 4.1 Choice of flat beams

In the classical regime, the number of photons emitted per beam particle  $n_\gamma$  depends on the bunch charge and transverse dimensions:

$$n_\gamma \propto \Upsilon \frac{\sigma_z}{\gamma} \propto \frac{N}{\sigma_x + \sigma_y}. \quad (11)$$

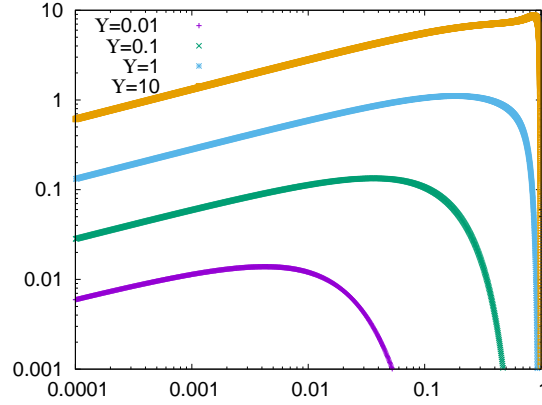


**Fig. 5:** The beamstrahlung power spectrum

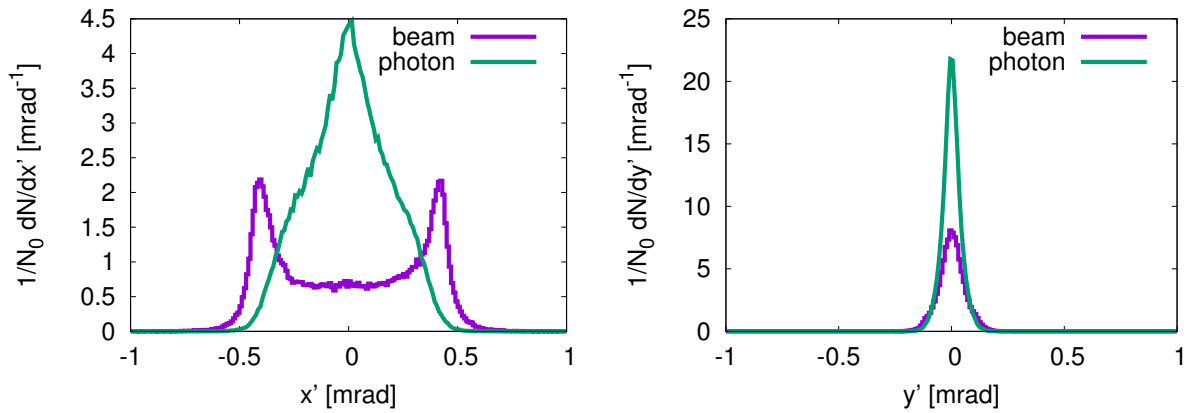


**Fig. 6:** The angular distribution of the spent beam including beamstrahlung

Similarly, the average energy  $E_\gamma$  of each photon is proportional to

$$E_\gamma \propto \Upsilon \frac{1}{\gamma} \propto \frac{N}{(\sigma_x + \sigma_y)\sigma_z}. \quad (12)$$

Typically, the emission of a single photon reduces the energy of the particle enough to not produce luminosity in the interesting energy range. Hence, the relevant parameter is the number of photons emitted rather than their energy.

For a given  $N$ , in order to reduce the beamstrahlung one thus aims to increase the sum of the transverse beam sizes  $\sigma_x + \sigma_y$ . At the same time the luminosity is proportional to  $1/(\sigma_x\sigma_y)$ , so one aims to minimize the product of the two beam sizes. Both goals can be simultaneously achieved by using a flat beam  $\sigma_x \gg \sigma_y$ ; the horizontal beam size is chosen to be larger than the vertical, since the damping rings naturally deliver a horizontal emittance that is larger than the vertical. For  $\sigma_x \gg \sigma_y$ , we can approximate  $\sigma_x \approx \sigma_x + \sigma_y$ . Hence, the term  $N/\sigma_x$  in Eq. (3) is proportional to the number of beamstrahlung photons.

## 4.2 Luminosity spectrum and choice of horizontal beam size

A lower limit of horizontal beam size and beta function arises from the beamstrahlung to limit the degradation of the luminosity spectrum. It is important to note that the luminosity spectrum is also affected by another process. If particles collide, they can emit a photon just before the collision as a part of the physics process; this is called initial state radiation. This emission is a radiative correction to the physics process. In contrast to beamstrahlung, it therefore happens only to colliding particles that undergo some

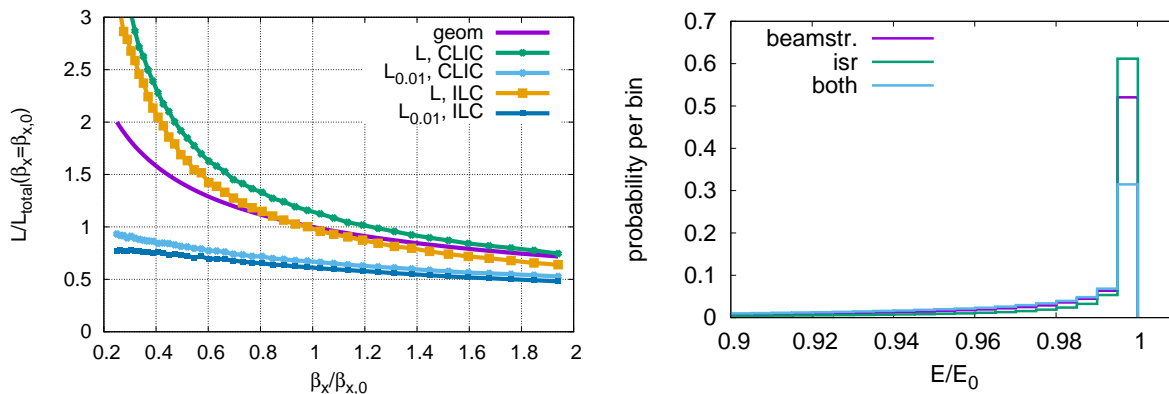


**Fig. 7:** Left: the total luminosity  $\mathcal{L}$  and the luminosity above 99% of the nominal energy  $\mathcal{L}_{0.01}$  as a function of the horizontal beta function. The beta function is normalized to the chosen value  $\beta_{x,0}$ . The curve labelled ‘geom’ neglects the beam–beam forces; in this case no beamstrahlung is emitted and the two luminosities are identical. Right: the luminosity spectrum in CLIC at 380 GeV. For comparison the spectra are also given taking into account only initial state radiation (isr) and only beamstrahlung.

physics process. However, it will degrade the luminosity spectrum in a similar fashion to beamstrahlung; the typical centre-of-mass energy spectrum of the colliding electrons and positrons is shown on the right-hand side of Fig. 7. Usually the experiments require that the degradation of the luminosity spectrum due to beamstrahlung is similar to the degradation due to initial state radiation. As a measure, one uses the ratio of the luminosity  $L_{0.01}$ , i.e. the part above 99% of the nominal centre-of-mass energy, and the total luminosity. In case of CLIC at 380 GeV a ratio of 60% has been targeted.

The total and peak luminosities are shown in Fig. 7 for CLIC and ILC as a function of the horizontal beta function. One can observe that the total luminosity increases strongly for smaller beta functions. It increases even faster than the geometric luminosity. This is a result of the fact that a smaller horizontal beam size increases the disruption and therefore leads to an increase in the pinch enhancement factor  $H_D$ . However, the peak luminosity only increases slightly for smaller beam sizes. Hence, the ratio of peak to total luminosity decreases rapidly for small beta functions, which yields a lower limit. It should be noted that additional lower limits for the horizontal beta function exist, e.g. from the ability to design the beam delivery system. With the chosen value, CLIC indeed reaches a ratio of 60%, as one can see on the right-hand side of Fig. 7.

In case of CLIC at 3 TeV, the requirement on the spectrum quality is somewhat relaxed (30%), since the tail of the luminosity spectrum also contributes to the creation of interesting physics events. An important example is the double-Higgs production, which allows us to measure the Higgs self-coupling. Basically the whole luminosity spectrum contributes to this production process at high energies, which increases the importance of the total luminosity with respect to the peak luminosity.

### 4.3 Choice of vertical beta function

The beam size at the collision point decreases as the beta function decreases proportionally to  $\sqrt{\beta_y}$ . However, the beam size just around the collision point increases faster as the beta function decreases. At any point  $s$  around the collision point  $s = 0$ , the beam size is proportional to

$$\sigma_y(s) \propto \sqrt{\beta(0) + \frac{s^2}{\beta(0)}}. \quad (13)$$

This hourglass effect limits the luminosity that one can gain by reducing the beta function; it is illustrated in Fig. 8. In the figure the luminosity is also shown as a function of the vertical beta function for the case

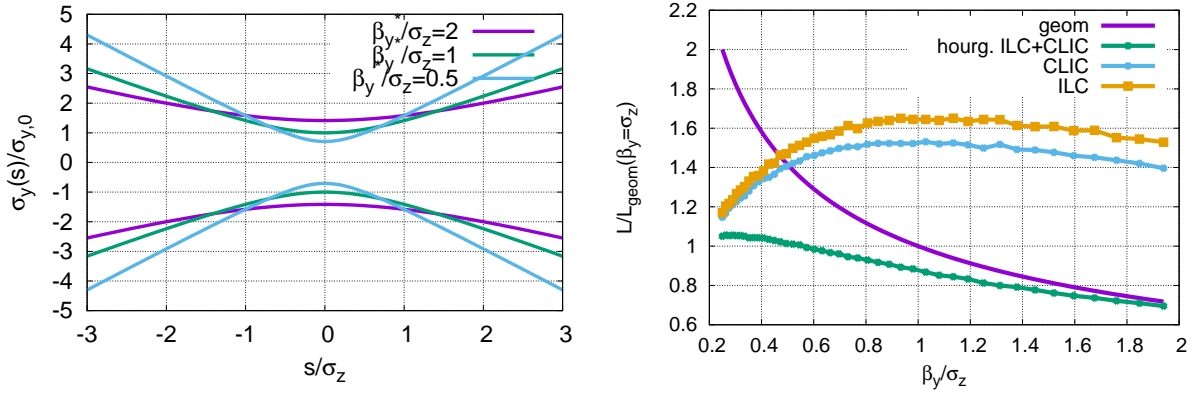


**Fig. 8:** Left: the beam size around the collision point for different beta functions. Right: the dependence of the luminosity on the vertical beta function. The curve labelled ‘geom’ indicates the dependence neglecting the hourglass effect.

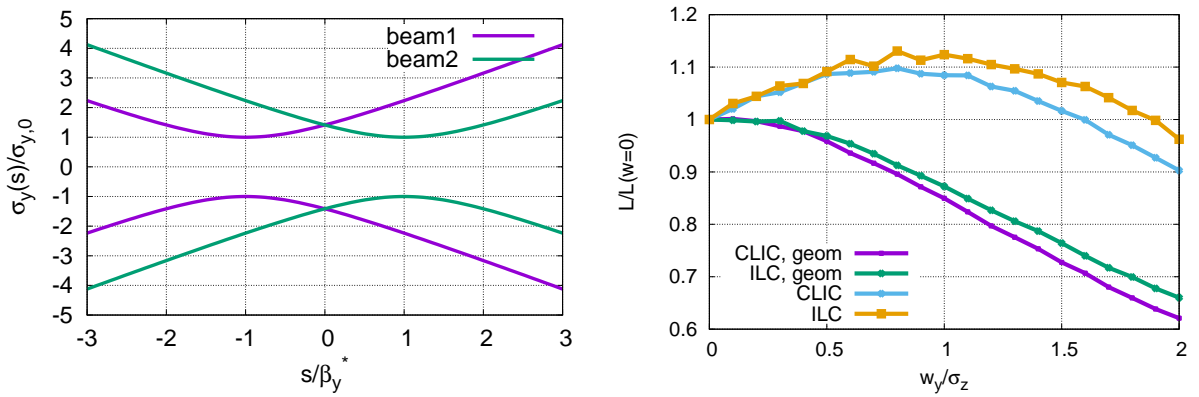


**Fig. 9:** Left: the beam size around the collision point for a waist before the collision point. Beam 1 comes from the left, beam 2 from the right. Right: the dependence of the luminosity on the vertical waist position. For the curve labelled ‘geom’ the beam–beam forces are neglected.

without beam–beam forces. As can be seen, the optimum beta function is about a quarter of the bunch length and the optimum is quite flat.

The dependence of the luminosity on the beta function is strongly modified by the beam–beam forces; see Fig. 8. For larger beta functions the pinch effect is more efficient in increasing the luminosity, moving the optimum choice to roughly  $\beta_y \approx \sigma_z$ . Obviously, the value depends on the strength of the beam–beam forces. For both projects a vertical beta function somewhat larger than the optimum has been chosen,  $\beta_y = 1.6 \sigma_z$  in ILC and  $\beta_y = 1.4 \sigma_z$  in CLIC. These choices lead to a very minor loss of luminosity. The larger beta function helps to ease the design of the beam delivery system.

#### 4.4 Waist shift

If the beam–beam forces are weak the maximum luminosity is obtained if the waists of the two beams are placed at the collision point. A distance  $W_y$  of the waists to the collision point leads to a reduced luminosity. Figure 9 shows the relative luminosity as a function of the waist position for ILC and CLIC if beam–beam forces are neglected. The dependence on  $W_y/\sigma_z$  differs slightly, since the ratio  $\beta_y/\sigma_z$  differs. If the beam–beam forces are taken into account the situation changes significantly. The maximum luminosity is obtained if the waists are positioned before the collision point,  $W_y > 0$ . For the optimum

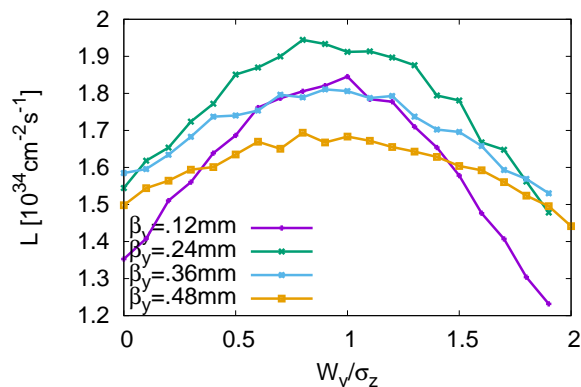


**Fig. 10:** The luminosity in ILC as a function of the waist shift for different beta functions

$W_y \approx \sigma_z$ , the luminosity is increased by 10% instead of the expected reduction of 10%.

In principle a full optimization of the vertical beta function and waist position can be performed. Figure 10 shows the results for ILC. The highest luminosity would be achieved using  $\beta_y \approx 0.24$  mm. It is interesting to note that using  $\beta_y \approx 0.48$  mm yields more luminosity than  $\beta_y \approx 0.12$  mm if the waists are at the collision point. But if the waist position is adjusted for maximum luminosity, the smaller beta function obtains more luminosity.

#### 4.5 Note on crossing angle

The beams in a linear collider cross with an angle in the horizontal plane,  $\theta_c = 14$  mrad in ILC and  $\theta_c = 20$  mrad in CLIC. This angle would reduce the luminosity to

$$\mathcal{L} = H_D \frac{N^2}{4\pi\sigma_x\sigma_y} n_b f_r \frac{1}{\sqrt{1 + \left(\frac{\sigma_z}{\sigma_x} \tan \frac{\theta_c}{c}\right)^2}}. \quad (14)$$

The reduction is about an order of magnitude. Therefore, crab cavities are used to rotate the bunches such that they collide head-on, even if their trajectories cross at an angle. One can thus ignore the crossing angle and assume that the collisions are head-on.

## 5 Imperfect collisions

The strong beam–beam forces change the dependence of the luminosity on the beam–beam offset. They can also lead to strong luminosity loss due to correlations in the longitudinal and transverse profiles.

### 5.1 Beam–beam offsets

If the beams are separated in the collision point, the luminosity is reduced. For rigid beams and neglecting the hourglass effect, the luminosity ratio can be described as a function of the offset  $\Delta y$  as

$$\frac{\mathcal{L}}{\mathcal{L}_0} = \exp\left(-\frac{\Delta y^2}{4\sigma_y^2}\right). \quad (15)$$

The beam–beam forces strongly modify this behaviour. Figure 11 shows the luminosity ratio as a function of offset for different disruption parameters. For weak disruption the luminosity decreases more slowly with offset than for rigid beams. For larger disruption very small offsets can lead to a large loss of luminosity. This is due to the fact that the collision becomes unstable, the kink instability, which is

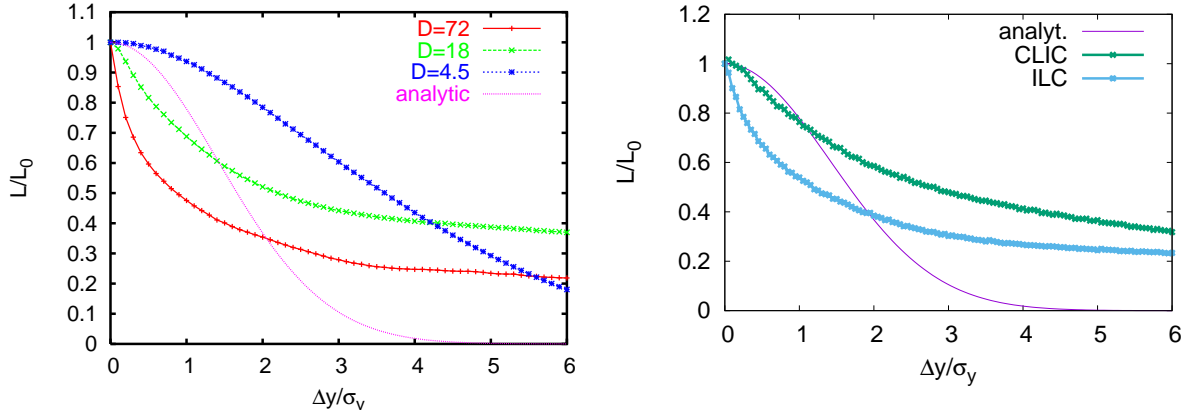


**Fig. 11:** Left: the luminosity ratio as a function of the offset for different disruption parameters. Right: the luminosity ratio as a function of vertical beam offset for ILC and CLIC.

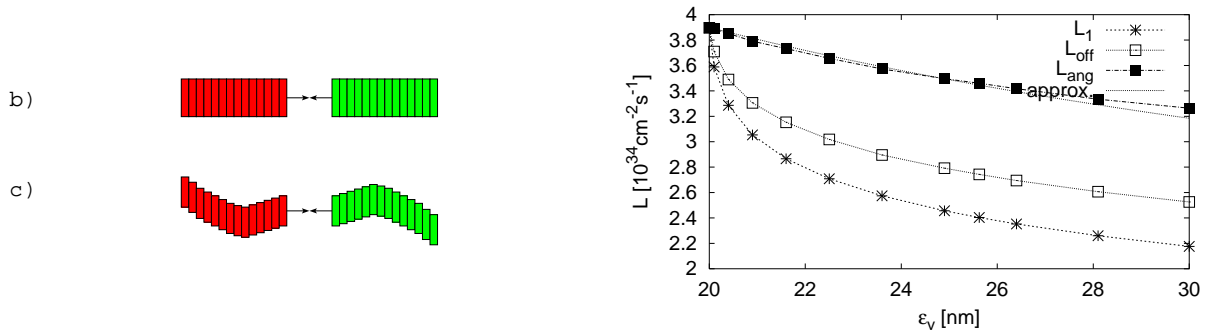


**Fig. 12:** Left: sketch of the emittance growth in the main linac due to wakefields and dispersion and the possible translations into beam shapes at the interaction point. Right: luminosity as a function of the emittance in the case of TESLA.

a typical two-stream instability. For large offsets, the beam–beam forces maintain more luminosity than for rigid beams. This is because the beams attract each other.

In order to avoid luminosity reduction a control of the beam–beam offset is required at the level of a fraction of a nanometre. The motion of the ground and vibrations of technical components make this a challenging task. Two main methods are used to address this challenge. First, in case of CLIC, the beam-guiding magnets are stabilized with active feedback systems that sense the motion of the magnet and correct it using movers. Second, in both ILC and CLIC, the beam–beam offset is measured and corrected with a beam-based feedback system. In case of ILC this feedback system can correct from one bunch to the next within the pulse; in CLIC it has a latency of a few bunch crossings and mainly acts from one pulse to the next. This feedback can easily detect an offset even of a fraction of a nanometre, since the resulting deflection of the beams is in the order of tens of  $\mu\text{rad}$ . A few metres downstream of the collision point such an angle has translated into an offset that can be easily measured with a beam position monitor.

### 5.2 The banana effect

Up to now we considered that the beam particles are independently distributed in the different dimensions and that there are no correlations. In practice one has to take correlations into account, i.e. to model the beam including the effects before the interaction point. This is particularly important if the vertical disruption is larger than about 15.

A good example of the importance of the integration of different subsystems is the so-called banana effect [11]. This effect has initially been studied for an older linear collider design, TESLA, but is also important for ILC. In early studies the emittance growth in the main linac was studied independently from the beam–beam simulations. However, wakefield effects in the main linac introduced correlated offsets (i.e. the mean vertical particle position depends on the longitudinal position within the bunch  $y(z)$ ), see c) on the left-hand side of Fig. 12. The projected emittance has then been used as input for the beam–beam simulations as in b). Instead simulations with full correlation should have been used as in c).

Systematic studies showed that the luminosity drops much faster with increasing beam emittance if the correlations are used in simulations than anticipated from the projected emittances [13]. This is shown on the right-hand side of Fig. 12. The horizontal scale indicates the emittance at the interaction point. The emittance consists of an uncorrelated part of 20 nm and an additional contribution from the wakefields in the main linac. The luminosity is shown on the vertical axis. The approximation assumes that the luminosity scales with  $1/\sigma_y$  and that the correlations are not relevant. The curve  $L_1$  shows the luminosity if both beams are centred in position and angle. Evidently the luminosity is very strongly affected by the emittance growth due to the wakefields. This is because the collision is unstable as a result of the high disruption.

The luminosity can be recovered if a full luminosity optimization is performed at the interaction point by varying the beam–beam offset ( $L_{\text{off}}$ ) and by varying offset and angle ( $L_{\text{ang}}$ ). This procedure however requires that the luminosity is measured online. Hence, it takes much more time than a simple beam position monitor-based feedback. In ILC it is foreseen to perform such an optimization during each bunch train. For a smaller disruption, as in CLIC, the banana effect is negligible. Hence, a luminosity optimization scan during the train is not required.

## 6 Beam–beam background and its impact on the detector design

The beam–beam effects lead to the generation of background for the physics experiments. This includes the production of electrons, positrons, muons and hadrons. In this lecture we will only discuss the production of electron–positron pairs, which have an important impact on the detector design.

### 6.1 Coherent pair creation

If the fields of the beams are very strong they can rip up the beamstrahlung photons, forming an electron–positron pair. This is called coherent pair creation, since it is caused by the beamstrahlung photons interacting with the coherent field of the beams, not by interacting with individual photons [14]. For  $\Upsilon \ll 1$ , almost no coherent pair creation exists. For larger values it becomes substantial. Both GUINEA-PIG and CAIN allow us to simulate the effect.

For the lower energy linear colliders coherent pair creation does not play an important role. For CLIC at 3 TeV the creation of pairs from beamstrahlung is significant. About  $6.8 \times 10^8$  pairs are produced per bunch crossing. The total charge of the pairs is hence about 20% of the beam charge. The spectrum of the pairs is shown in Fig. 13; the average particle energy is about 300 GeV. The pair particles are produced at very small angles. However, a produced electron can move in the direction of the electron beam or in the direction of the positron beam. In the first case it is focused by the oncoming positron beam and in the second case it is defocused by the oncoming electron beam. It can then be deflected to larger angles. The equivalent is true for the produced positrons. It is therefore important that the detector provides a large enough acceptance in the outgoing beamline to avoid excessive losses from coherent pairs. In Fig. 14, the total powers above a certain angle are shown for the spent beam, the beamstrahlung photons and the coherent pairs. As can be seen, an exit aperture of about 10 mrad is well sufficient to avoid losses of more than 1 W in the detector. It should be noted that 1 W corresponds to a total energy of 400 TeV per bunch crossing or roughly the energy of 300 beam particles.

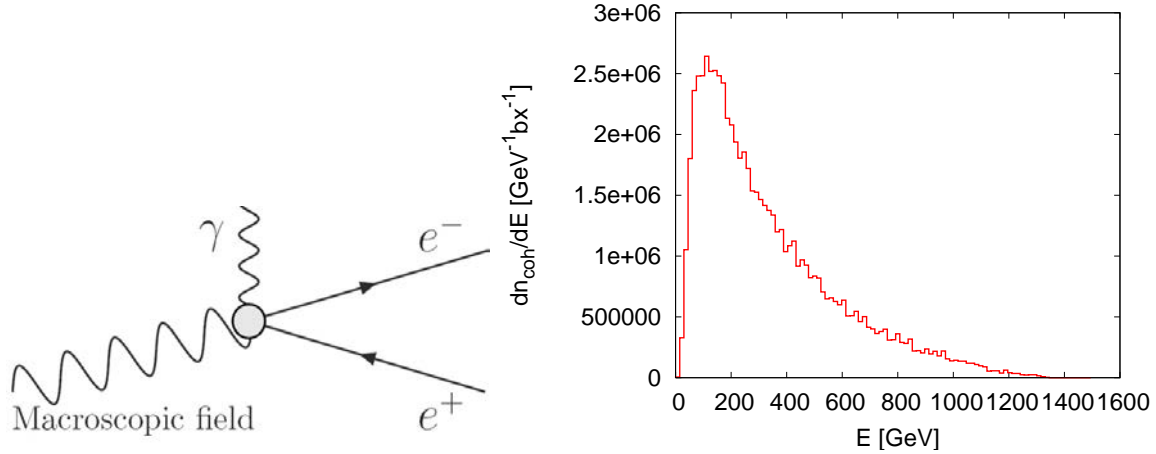


**Fig. 13:** Left: the Feynman diagram for the coherent pair creation. Right: the energy spectrum of the coherent pairs in CLIC at 3 TeV.

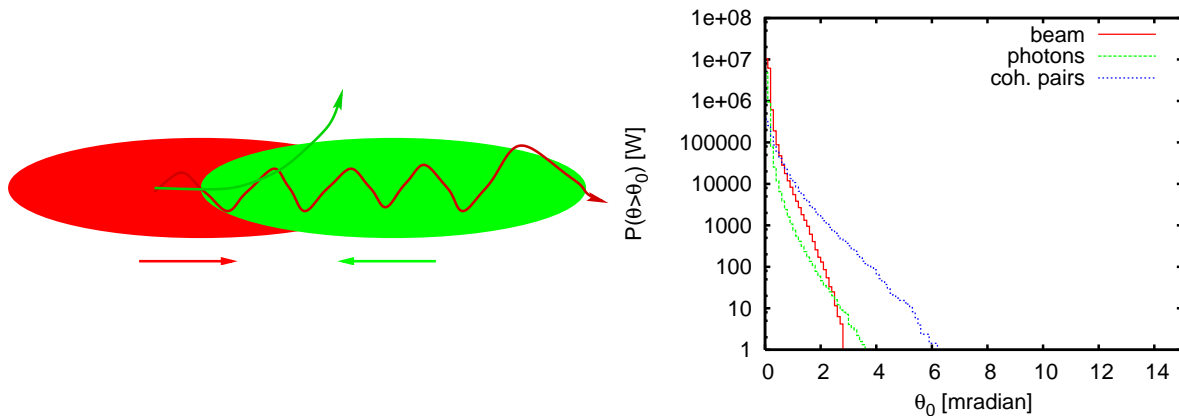


**Fig. 14:** Left: the particle from coherent pair creation can be focused or defocused by the beams. Right: the total power in the spent beam above a given angle in the case of CLIC at 3 TeV.

It should be noted that not only the real photons from beamstrahlung can be turned into pairs. If the field is strong enough, even the virtual photons that are co-moving with the beam particles can be turned into pairs. This is called the trident cascade process, because a single electron or positron generates an additional pair in the external field. For  $\Upsilon \gg 1$ , the trident cascade becomes a large source of pairs. This is particularly problematic because the beam particles can lose a large part of their energy in this process, degrading the luminosity spectrum. In the present linear collider designs the trident cascade process does not play an important role. At higher energies or with shorter bunches it would become substantial. GUINEA-PIG++ allows us to simulate the trident cascade process.

## 6.2 Incoherent pair creation

Colliding photons can turn into an electron–positron pair. In linear colliders two main sources of these photons exist. One is the above-mentioned beamstrahlung. The other are virtual photons that accompany each electron and positron. As a consequence three production mechanisms of pairs exist: the Breit–Wheeler process (two real photons form a pair), the Bethe–Heitler process (one real and one virtual photon form a pair) and the Landau–Lifshitz process (two virtual photons form a pair). The most fundamental Feynman graphs are shown in Fig. 15. It is interesting to note that the actual calculation of the pair production is complicated by the so-called beam-size effect. That is, that the size of the

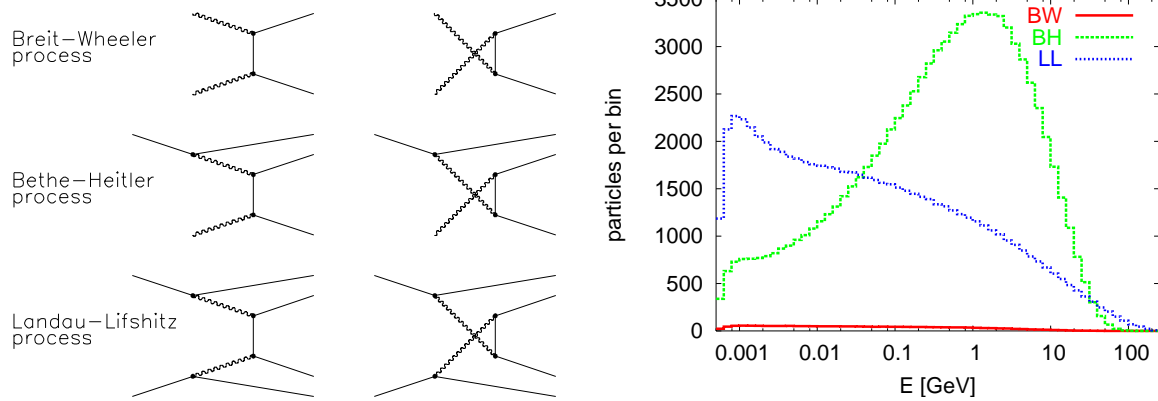


**Fig. 15:** Left: the Feynman diagrams for the incoherent pair creation. Right: the energy spectrum of the incoherent pairs for an older CLIC design at 500 GeV.

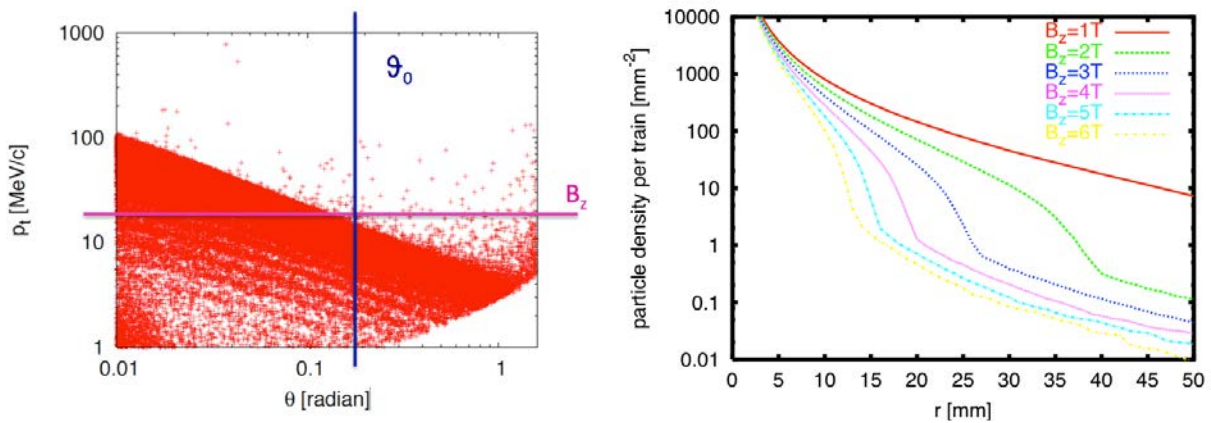


**Fig. 16:** Left: the angle and transverse momentum of incoherent particles after the beam collision. Right: the number of hits in the vertex detector as a function of the detector radius and for different detector main solenoid fields.

beam modifies the cross-section. In addition the strong fields of the beams also modify the cross-section. Conventional programs that simulate pair production do not take these effects into account. However, GUINEA-PIG and CAIN can model these effects. Typically the number of pairs is  $O(10^5)$  per bunch crossing; see Table 1. An example spectrum can be seen in Fig. 15.

Some of the incoherent pair particles are produced at larger angles, but most are produced at small angles. The pairs are deflected in the same fashion as the coherent pairs. However, the deflection is more important because the energy of the incoherent pairs is typically smaller. Pair particles can therefore be deflected to relatively large angles. The maximum deflection is given by the particle energy. An example of the final transverse momentum and angle of the pair particles is shown in Fig. 16. One can see the few particles that have been produced at large angles. The sharp edge in the plot corresponds to the maximum deflection that a pair particle of a given energy can obtain from the beams.

The most important effect of the incoherent pairs is that the particles can hit the vertex detector that is as close to the beam as reasonably possible (typically a couple of centimetres). This detector identifies the origin of particles in the detector. It can determine whether a track originates directly from the colliding beams or if it starts at some distance from the beams because it is produced by a decay product of a particle.

A significant number of background electrons and positrons hitting this detector will compromise its performance. The impact of these particles on the detector is suppressed by two measures. First, the detector solenoid field forces particles on a helical trajectory. The radius of the helix is given by the transverse momentum and hence particles with small  $p_{\perp}$  will not hit the detector. Second, particles at small angles will also not hit the detector. The number of hits in a vertex detector of fixed angular coverage is shown in Fig. 16 for different detector solenoid fields. As the radius of the vertex detector increases, the number of hits decreases and they are distributed over a larger area. The relatively steep edge corresponds to the maximum deflection of the pairs by the beams. One typically chooses a radius sufficiently larger than the edge to guarantee good detector performance. Here, the detector design is a direct consequence of the beam-beam effect and the corresponding background.

## 7 Conclusion

Beam-beam effects are important drivers for linear collider designs. The beamstrahlung is one of the main limitations for the luminosity and affects the capabilities of the experiments. Background from the beam-beam interaction also impacts the detector design, in particular the choice of beam-pipe radius. It also affects the low-angle detector design.

## References

- [1] N. Phinney, SLC final performance and lessons, eConf C **00082** (2000) MO102 [physics/0010008 [physics.acc-ph]].
- [2] T. Behnke *et al.*, The international linear collider technical design report – Vol. 1: Executive summary, arXiv:1306.6327 [physics.acc-ph] (2013).
- [3] H. Baer *et al.*, The international linear collider technical design report – Vol. 2: Physics, arXiv:1306.6352 [hep-ph] (2013).
- [4] C. Adolphsen *et al.*, The international linear collider technical design report – Vol. 3.I: Accelerator R&D in the technical design phase, arXiv:1306.6353 [physics.acc-ph] (2013).
- [5] C. Adolphsen *et al.*, The international linear collider technical design report – Vol. 3.II: Accelerator baseline design, arXiv:1306.6328 [physics.acc-ph] (2013).
- [6] T. Behnke *et al.*, The international linear collider technical design report – Vol. 4: Detectors, arXiv:1306.6329 [physics.ins-det] (2013).
- [7] M. Aicheler *et al.*, A multi-TeV linear collider based on CLIC technology: CLIC conceptual design report (2012). <http://dx.doi.org/10.5170/CERN-2012-007>
- [8] L. Linssen, A. Miyamoto, M. Stanitzki and H. Weerts, Physics and detectors at CLIC: CLIC conceptual design report, arXiv:1202.5940 [physics.ins-det] (2012). <http://dx.doi.org/10.5170/CERN-2012-003>
- [9] P. Chen, G. Horton-Smith, T. Ohgaki, A.W. Weidemann and K. Yokoya, CAIN: Conglomerat d'ABEL et d'interactions nonlineaires. SLAC-PUB-6583 (1995).
- [10] D. Schulte, Electronmagnetic and Hadronic Background in the Interaction Region of the TESLA Collider. DESY-TESLA-97-08 (1997).
- [11] R. Brinkmann, O. Napoly and D. Schulte, Beam-beam instabilities driven by wakefield effects in the main linac, PAC-2001-TPPH153 (2001).
- [12] D. Schulte, Luminosity in future linear collider in the presence of static wakefield effects in the main linac, CLIC-Note-544 (2002).
- [13] D. Schulte, An update on the banana effect, Nanobeam 2002 and CERN-AB-2003-009 (2003).
- [14] P. Chen and V. Telnov, *Phys. Rev. Lett.* **63** (1990) 1796. <http://dx.doi.org/10.1103/physrevlett.63.1796>